Available online at www.sciencedirect.com
SCIENCE DIRECT®
International Journal of Mass Spectrometry 227 (2003) 1–20
International Journal of Mass Spectrometry
www.elsevier.com/locate/ijms

Cation-π interactions with a model for an extended π network Absolute binding energies of alkali metal cation–naphthalene complexes determined by threshold collision-induced dissociation and theoretical studies

R. Amunugama, M.T. Rodgers*

Department of Chemistry, Wayne State University, Detroit, MI 48202, USA

Received 14 August 2002; accepted 7 October 2002

In honor of R.C. Dunbar on the occasion of his 60th birthday, a great friend and gas-phase ion chemist.

Abstract

Threshold collision-induced dissociation (CID) techniques are employed to determine the bond dissociation energies (BDEs) of both mono and bis cation-π complexes of the alkali metal cations (Li^+, Na^+, K^+, Rb^+, and Cs^+) with naphthalene ($C_{10}H_8$). The primary and lowest energy dissociation channel observed in all cases is endothermic loss of an intact naphthalene ligand. Sequential dissociation of a second naphthalene ligand is observed at elevated energies in the bis complexes. The ligand exchange products, M^+Xe and $M^+(C_{10}H_8)Xe$, are also observed in minor yield. Density functional theory calculations at the B3LYP/6-31G* level of theory are used to determine the structures, vibrational frequencies, and rotational constants of these complexes and their primary dissociation products. Theoretical binding energies are determined from single point energy calculations at the MP2(full)/6-311+G(2d,2p) level using the B3LYP/6-31G* geometries. The agreement between theory and experiment is reasonably good for the Li^+, Na^+, and K^+ complexes where full electron correlation is included, except for the $Li^+(C_{10}H_8)$ complex. Somewhat less satisfactory agreement is found for the Rb^+ and Cs^+ complexes where effective core potentials (ECPs) are used. The trends in the BDEs of these complexes to naphthalene as well as those to other π ligands previously examined, aniline, anisole, benzene, fluorobenzene, phenol, and toluene, confirm the noncovalent nature of the bonding in such cation-π complexes. Comparisons amongst these π ligands are made to examine the influence of the extended π network on the binding and the factors that control the strength of cation-π interactions.

Keywords: Alkali metal ions; Bond dissociation energies; Cation-π interactions; Collision-induced dissociation; Guided ion beams

1. Introduction

The three-dimensional structures of biological macromolecules are determined by a delicate balance of weak noncovalent interactions. Noncovalent interactions, such as hydrogen bonds, salt bridges, and hydrophobic interactions, are generally referred to as classical noncovalent interactions because their importance in determining the structure and influencing the function of biological systems has long been recognized. The importance of other noncovalent

* Corresponding author. Tel.: +1-313-577-2431; fax: +1-313-577-8822.
E-mail address: mrodgers@chem.wayne.edu (M.T. Rodgers).

1387-3806/03/$ – see front matter © 2003 Elsevier Science B.V. All rights reserved.
doi:10.1016/S1387-3806(03)00039-3

interactions, such as cation-π [1,2] charge-dipole [3,4] and π-stacking [5,6] interactions, has only recently come to light. These noncovalent interactions are currently receiving a great deal of attention and are referred to as nonclassical noncovalent interactions. Cation-π interactions between a positively charged metal cation and an aromatic ligand with a delocalized π-electron cloud were first recognized and studied in the gas phase [7–11] However, biological implications of this strong cation-π interaction were recognized only after pioneering work by Ma and Dougherty [1] and Dougherty [2]. Today cation-π interactions are now believed to be crucial structural determinants in the folding and assembly of large systems [1,2,12–16], and are also believed to play a central role in the functioning of ionic channels in membranes [17,18] The binding of alkali metal cations, and in particular Na^+ and K^+, to the exposed π faces of aromatic amino acids that lie along the interior surfaces of ionic channels is thought to play a role in the selective transport of these metal cations through the ion channel [19,20]. Cation-π interactions operative in biological systems may involve monovalent or divalent atomic metal cations, or closed shell nonmetallic molecular cations, such as alkylammonium ions [1,2,21]. Cation-π interactions involving Na^+ and K^+, the most biologically relevant alkali metal cations, have been reported in the literature [1,21,22].

Knowledge of the structure and energetics of binding in small model systems can be used to gain a better understanding of the interaction of alkali metal cations to large biological molecules, such as proteins. Thus, characterizing these interactions in the gas phase is an important and essential part of building a database of information concerning the nature and strength of cation-π interactions and the influence of the local environment on such interactions. Experimental gas-phase studies have been carried out for a number of model systems: benzene [7,10,23–26], pyrrole [27,33], and their derivatives, such as toluene [29], fluorobenzene [30], aniline [31], phenol [32,33], anisole [34], and indole [33], as well as the aromatic amino acids [35,36]. Many of these gas-phase studies have been supported and enhanced by high-level theoretical calculations [1,25–34,37–39]. These model systems constitute the simplest groups of larger aromatic ligands that mimic the binding properties of π-donating ligands believed to participate in cation-π interactions operative in biological systems.

In an effort aimed at understanding the influence of the local environment on the strength of cation-π interactions, we set out to determine the absolute binding energies of alkali metal cations to a variety of aromatic ligands. Studies by Amicangelo and Armentrout [26] had previously examined benzene. Our earlier work expanded on this by examining the influence of various substituents, such as methyl [29], amino [31], hydroxyl [32], methoxy [34], and fluoro [30], on the strength of cation-π interactions. In the present study, we extend these studies to include a model system for an extended π network by examining cation-π interactions between the alkali metal cations, Li^+, Na^+, K^+, Rb^+, and Cs^+, and naphthalene, $C_{10}H_8$. Naphthalene is a good model to mimic the behavior of tryptophan [40], one of the commonly occurring aromatic amino acids, as well as biological assemblies containing extended π networks. Previous investigations of cation-π interactions involving naphthalene have been somewhat limited. Only two theoretical studies have been reported. In the first study by Mecozzi et al. [39], the binding energy of a variety of aromatic ligands, including naphthalene, to Na^+ was examined. The second study involved an ab initio mapping study of the interactions of naphthalene and tryptophan with Na^+, Mg^+, and Al^+ [40]. The only experimental work reported involving cation-π interactions with naphthalene is a study in which Dunbar et al. [41] examined the radiative association reactions of Si^+, Fe^+, Cr^+, and Mn^+ with naphthalene.

The kinetic energy-dependent cross-sections for the primary collision-induced dissociation (CID) process observed for each $M^+(C_{10}H_8)_x$ complex are analyzed using methods developed previously [42]. The analysis explicitly includes the effects of the internal and translational energy distributions of the reactants, multiple ion-neutral collisions, and the lifetime for dissociation. We derive M^+–$C_{10}H_8$, and $(C_{10}H_8)M^+$–$C_{10}H_8$ bond dissociation energies (BDEs) for all five of the alkali

metal cations and compare these results to ab initio and density functional calculations performed here and in the literature [39,40]. Comparisons are also made to the analogous benzene [26], toluene [29], fluorobenzene [30], aniline [31], phenol [32], and anisole [34] systems studied previously to examine the influence of the extended π network on the binding, and the factors that control the strength of cation-π interactions.

2. Experimental section

2.1. General procedures

A guided ion beam tandem mass spectrometer that has previously been described in detail [43] was used to measure the absolute CID cross-sections of the cation-π complexes, $M^+(C_{10}H_8)$ and $M^+(C_{10}H_8)_2$, where $M^+ = Li^+$, Na^+, K^+, Rb^+, and Cs^+. The complexes are generated in a flow tube ion source by condensation of the alkali metal cation and neutral naphthalene molecule(s). The complexes are collisionally stabilized and thermalized by $\sim 10^5$ collisions with the He and Ar bath gases such that the internal energies of the ions emanating from the source region are well described by a Maxwell–Boltzmann distribution at room temperature [43]. The ions are extracted from the source, accelerated, and focused into a magnetic sector momentum analyzer for mass analysis. Mass-selected ions are decelerated to a desired kinetic energy and focused into an octopole ion guide. The octopole passes through a static gas cell containing Xe at low pressures (0.05–0.20 mTorr), to ensure that multiple ion-neutral collisions are unlikely. The octopole ion guide acts as an efficient trap for ions in the radial direction. Therefore, loss of scattered reactant and product ions in the octopole region is almost entirely eliminated [44]. These ions drift to the end of the octopole where they are focused into a quadrupole mass filter for mass analysis, and subsequently detected with a secondary electron scintillation detector and standard pulse counting techniques.

Ion intensities are converted to absolute cross-sections using a Beer's law analysis [45]. Errors in the pressure measurement and the length of the interaction typically result in absolute uncertainties of ±20% in cross-section magnitudes. Relative uncertainties are approximately ±5%. Because very light mass ions, such as Li^+, are not trapped in the octopole with high efficiency, absolute uncertainties in the magnitudes of the cross-sections for Li^+ products are ±50%.

Ion kinetic energies in the laboratory frame, E_{lab}, are converted to energies in the center-of-mass (CM) frame, E_{CM}. All energies reported below are in the CM frame unless otherwise noted. The absolute zero and distribution of the ion kinetic energies are determined using the octopole ion guide as a retarding potential analyzer as previously described [45]. The distribution of ion kinetic energies is nearly Gaussian with a fwhm between 0.2 and 0.4 eV (lab) for these experiments. The uncertainty in the absolute energy scale is ±0.05 eV (lab).

Pressure-dependent studies of all cross-sections examined here were performed because multiple collision can influence the shape of CID cross-sections and the threshold regions are most sensitive to these effects. Data free from pressure effects are obtained by extrapolating to zero reactant pressure, as described previously [46]. Results reported below are, therefore, due to single bimolecular encounters.

2.2. Thermochemical analysis

The threshold regions of the reaction cross-sections are modeled using Eq. (1),

$$\sigma(E) = \sigma_0 \sum_i g_i (E + E_i - E_0)^n / E \quad (1)$$

where σ_0 is an energy-independent scaling factor, E is the relative translational energy of the reactants, E_0 is the threshold for reaction of the ground electronic and ro-vibrational state, and n is an adjustable parameter that describes the efficiency of collisional energy transfer [47]. The summation is over the ro-vibrational states of the reactant ions, i, where E_i is the excitation energy of each ro-vibrational state and g_i is the population of those states ($\sum g_i = 1$). The populations of excited ro-vibrational levels are not negligible

even at 298 K as a result of the many low-frequency modes present in these ions. The relative reactivity of all ro-vibrational states, as reflected by σ_0 and n, is assumed to be equivalent.

The Beyer–Swinehart algorithm [48] is used to evaluate the density of the ro-vibrational states, and the relative populations, g_i, are calculated by an appropriate Maxwell–Boltzmann distribution at the 298 K temperature appropriate for the reactants. The vibrational frequencies of the reactant complexes are determined from density functional theory calculations as discussed in Section 2.3. The average vibrational energy at 298 K of the $M^+(C_{10}H_8)_x$ complexes is given in Table 1. To account for the inaccuracies in the computed frequencies, we have increased and decreased the pre-scaled frequencies by 10% for the $M^+(C_{10}H_8)_x$ complexes to Li^+, Na^+, and K^+. This scaling procedure encompasses the range of scale factors needed to bring calculated frequencies into agreement with experimentally determined frequencies found by Pople et al. [49]. For the complexes to Rb^+ and Cs^+, 20% variations were applied. The corresponding change in the average vibrational energy is taken to be an estimate of one standard deviation of the uncertainty in vibrational energy (Table 1).

Statistical theories for unimolecular dissociation (Rice–Ramsperger–Kassel–Marcus (RRKM) theory) of the collisionally activated ions are also included in Eq. (1) to account for the possibility that these ions may not have undergone dissociation prior to arriving at the detector ($\sim 10^{-4}$ s, but energy dependent) [42,50]. Ro-vibrational frequencies appropriate for the energized molecules and the transition states (TSs) leading to dissociation are given in Tables 1 and 2. In our analysis, we assume that the TSs are loose and product-like because the interaction between the alkali metal cation and the naphthalene ligand(s) is largely electrostatic (ion-quadrupole and ion-induced dipole). The best model for the TS of such electrostatically bound complexes is a loose phase space limit (PSL) model located at the centrifugal barrier for the interaction of $M^+(C_{10}H_8)_{x-1}$ with $C_{10}H_8$ as described in detail elsewhere [42]. The TS vibrations appropriate for the PSL model are the frequencies of the products which are also found in Table 1. The transitional frequencies, those that become rotations of the completely dissociated products, are treated as rotors. The transitional mode rotors and the one-dimensional external rotor of the TS are simply the rotational constants of the molecular products(s) formed in the CID reaction as previously discussed in detail [42]. These are listed in Table 2. The two-dimensional external rotational constant of the TS is determined by assuming that the TS occurs at the centrifugal barrier for interaction of $M^+(C_{10}H_8)_{x-1}$ with the neutral $C_{10}H_8$ molecule, treated variationally as outlined elsewhere [42]. The two-dimensional external rotations are treated adiabatically but with centrifugal effects included using a statistical distribution with explicit summation over the possible values of the rotational quantum number, as described in detail elsewhere [42].

The model represented by Eq. (1) is expected to be appropriate for translationally driven reactions [51] and has been found to reproduce CID cross-sections well. The model is convoluted with the kinetic energy distributions of both the reactant ion and neutral Xe atom, and a nonlinear least-squares analysis of the data is performed to give optimized values for the parameters σ_0, E_0, and n. The error associated with the measurement of E_0 is estimated from the range of threshold values determined for different zero-pressure extrapolated data sets, variations associated with uncertainties in the vibrational frequencies (scaling as discussed above), and the error in the absolute energy scale, 0.05 eV (lab). For analyses that include the RRKM lifetime effect, the uncertainties in the reported E_0 values also include the effects of increasing and decreasing the time assumed available for dissociation ($\sim 10^{-4}$ s) by a factor of 2.

Eq. (1) explicitly includes the internal energy of the ion, E_i. All energy available is treated statistically because the internal (rotational and vibrational) energy of the reactants is redistributed throughout the ion in the collision with Xe. Because the CID processes examined here are simple noncovalent bond fission reactions, the E_0 values determined by analysis with Eq. (1) can be equated to 0 K BDEs [52,53].

Table 1
Vibrational frequencies and average vibrational energies at 298 K[a]

Species	E_{vib} (eV)[b]	Frequencies (cm^{-1})
$C_{10}H_8$	0.08 (0.02)	173, 186, 357, 389, 472, 483, 508, 510, 621, 623, 720, 761, 770, 788, 792, 836, 883, 929, 931, 945, 966, 975, 1024, 1035, 1135, 1158, 1161, 1171, 1219, 1252, 1271, 1382, 1389, 1403, 1477, 1480, 1537, 1598, 1626, 1655, 3114, 3116, 3117, 3121, 3132, 3133, 3145, 3146
$Li^+(C_{10}H_8)$	0.19 (0.02)	**146**, **157**, 245, 261, 356, **378**, 395, 465, 491, 506, 509, 612, 618, 748, 751, 753, 789, 820, 863, 904, 932, 966, 982, 995, 1009, 1014, 1029, 1133, 1160, 1167, 1178, 1218, 1251, 1270, 1361, 1385, 1399, 1465, 1472, 1518, 1580, 1598, 1637, 3140, 3143(2), 3145, 3158(2), 3167, 3168
$Na^+(C_{10}H_8)$	0.21 (0.02)	**71**, **91**, 187, 193, **203**, 356, 389, 469, 488, 506, 508, 616, 619, 742, 752, 761, 789, 811, 856, 896, 930, 958, 973, 988, 1003, 1014, 1030, 1133, 1159, 1163, 1176, 1216, 1250, 1269, 1365, 1381, 1400, 1467, 1473, 1523, 1583, 1607, 1639, 3131, 3133, 3136, 3138, 3148, 3154, 3158, 3165
$K^+(C_{10}H_8)$	0.22 (0.02)	**48**, **74**, **136**, 187, 193, 356, 389, 470, 489, 506, 509, 616, 620, 740, 754, 759, 789, 807, 854, 892, 929, 954, 969, 986, 998, 1017, 1031, 1134, 1159, 1163, 1175, 1216, 1251, 1270, 1372, 1380, 1401, 1469, 1475, 1526, 1587, 1614, 1643, 3125, 3128, 3131, 3133, 3143, 3150, 3155, 3162
$Rb^+(C_{10}H_8)$	0.22 (0.04)	**41**, **64**, **117**, 187, 193, 356, 389, 470, 489, 506, 509, 616, 620, 740, 754, 759, 789, 807, 854, 892, 929, 954, 969, 986, 998, 1017, 1031, 1134, 1159, 1163, 1175, 1216, 1251, 1270, 1372, 1380, 1401, 1469, 1475, 1526, 1587, 1614, 1643, 3125, 3128, 3131, 3133, 3143, 3150, 3155, 3162
$Cs^+(C_{10}H_8)$	0.22 (0.04)	**39**, **61**, **112**, 187, 193, 356, 389, 470, 489, 506, 509, 616, 620, 740, 754, 759, 789, 807, 854, 892, 929, 954, 969, 986, 998, 1017, 1031, 1134, 1159, 1163, 1175, 1216, 1251, 1270, 1372, 1380, 1401, 1469, 1475, 1526, 1587, 1614, 1643, 3125, 3128, 3131, 3133, 3143, 3150, 3155, 3162
$Li^+(C_{10}H_8)_2$	0.45 (0.04)	**12**, **15**, **35**, **45**, **53**, **92**, **155**, 166, 179, 189, 210, 219, 356, 356, **370**, 386, 387, 466, 467, 485, 487, 506(2), 509(2), 615(2), 619, 620, 739, 743, 754, 755, 760, 762, 790(2), 809, 814, 853, 857, 894, 899, 931, 932, 956, 958, 971, 974, 985, 988, 999, 1000, 1016, 1018, 1030, 1031, 1133, 1135, 1159, 1160, 1164, 1165, 1175, 1176, 1217, 1219, 1252(2), 1252, 1270, 1271, 1369, 1370, 1386, 1387, 1400, 1401, 1469(2), 1473, 1474, 1524(2), 1585, 1586, 1608, 1609, 1643(2), 3134(2), 3136(2), 3137(2), 3139, 3140, 3151, 3152(3), 3161, 3162(2), 3163
$Na^+(C_{10}H_8)_2$	0.46 (0.04)	**8**, **20**, **21**, **35**, 56, **65**, **95**, **103**, 181, 186, 189, 193, **224**, 356(2), 389(2), 470(2), 487, 488, 507(2), 509(2), 618(2), 620(2), 737, 739, 754(2), 763, 764, 789, 790, 804, 808, 852, 854, 892, 894, 930(2), 953, 954, 967, 969, 984, 985, 998(2), 1016, 1017, 1031(2), 1134(2), 1159(2), 1163(2), 1175(2), 1216, 1217, 1251(2), 1270(2), 1369, 1370, 1382(2), 1401(2), 1469(2), 1474(2), 1525(2), 1586, 1587, 1611, 1612, 1643(2), 3128(2), 3131(2), 3132, 3133, 3135(2), 3145, 3146, 3150, 3151, 3156, 3157, 3162(2)
$K^+(C_{10}H_8)_2$	0.47 (0.04)	**4**, **12**, **13**, **31**, **45**, **59**, 74, **78**, **152**, 184, 186, 192(2), 356(2), 390(2), 471(2), 488, 489, 507(2), 509(2), 617(2), 620(2), 735, 737, 755(2), 761, 762, 790(2), 802, 804, 851, 852, 889, 891, 929(2), 950, 951, 965, 966, 983, 984, 995(2), 1018(2), 1031, 1032, 1134, 1135, 1159(2), 1162(2), 1174, 1175, 1216, 1217, 1252(2), 1270(2), 1374(2), 1381(2), 1401(2), 1471(2), 1475(2), 1527(2), 1589(2), 1615, 1616, 1645(2), 3124(2), 3127(2), 3129(2), 3131(2), 3143(2), 3148(2), 3154(2), 3160(2)
$Rb^+(C_{10}H_8)_2$	0.48 (0.08)	**3**, **10**, **11**, **27**, **45**, **59**, **74**, 78, **131**, 184, 186, 192(2), 356(2), 390(2), 471(2), 488, 489, 507(2), 509(2), 617(2), 620(2), 735, 737, 755(2), 761, 762, 790(2), 802, 804, 851, 852, 889, 891, 929(2), 950, 951, 965, 966, 983, 984, 995(2), 1018(2), 1031, 1032, 1134, 1135, 1159(2), 1162(2), 1174, 1175, 1216, 1217, 1252(2), 1270(2), 1374(2), 1381(2), 1401(2), 1471(2), 1475(2), 1527(2), 1589(2), 1615, 1616, 1645(2), 3124(2), 3127(2), 3129(2), 3131(2), 3143(2), 3148(2), 3154(2), 3160(2)
$Cs^+(C_{10}H_8)_2$	0.48 (0.09)	**3**, **10**, **11**, **25**, **45**, **59**, 74, **78**, **125**, 184, 186, 192(2), 356(2), 390(2), 471(2), 488, 489, 507(2), 509(2), 617(2), 620(2), 735, 737, 755(2), 761, 762, 790(2), 802, 804, 851, 852, 889, 891, 929(2), 950, 951, 965, 966, 983, 984, 995(2), 1018(2), 1031, 1032, 1134, 1135, 1159(2), 1162(2), 1174, 1175, 1216, 1217, 1252(2), 1270(2), 1374(2), 1381(2), 1401(2), 1471(2), 1475(2), 1527(2), 1589(2), 1615, 1616, 1645(2), 3124(2), 3127(2), 3129(2), 3131(2), 3143(2), 3148(2), 3154(2), 3160(2)

[a] Vibrational frequencies are obtained from a vibrational analysis of the B3LYP/6-31G* geometry-optimized structures for neutral $C_{10}H_8$ and $M^+(C_{10}H_8)_x$, where $M^+ = Li^+$, Na^+, and K^+, and scaled by 0.9804. For $M^+ = Rb^+$ and Cs^+, vibrational frequencies were estimated by scaling the calculated frequencies for the analogous $K^+(C_{10}H_8)_x$ complexes as described in the text. The metal–ligand stretches and bends, corresponding to the transitional modes, are indicated in bold typeface, where the largest of these frequencies is the reaction coordinate.

[b] Uncertainties listed in parentheses are determined as described in the text.

Table 2
Rotational constants of $M^+(C_{10}H_8)_x$ in cm^{-1}

Reactant	Energized molecule		Transition state		
	1-D[a]	2-D[b]	1-D[c]	2-D[c]	2-D[d]
$Li^+(C_{10}H_8)$	0.091	0.033	0.10	0.035	0.032
$Na^+(C_{10}H_8)$	0.064	0.029	0.10	0.035	0.0039
$K^+(C_{10}H_8)$	0.046	0.025	0.10	0.035	0.0013
$Rb^+(C_{10}H_8)$	0.046	0.025	0.10	0.035	0.0004
$Cs^+(C_{10}H_8)$	0.046	0.025	0.10	0.035	0.0003
$Li^+(C_{10}H_8)_2$	0.015	0.010	0.091, 0.10	0.033, 0.035	0.0006
$Na^+(C_{10}H_8)_2$	0.014	0.008	0.064, 0.10	0.029, 0.035	0.0006
$K^+(C_{10}H_8)_2$	0.014	0.006	0.046, 0.10	0.025, 0.035	0.0006
$Rb^+(C_{10}H_8)_2$	0.014	0.006	0.046, 0.10	0.025, 0.035	0.0004
$Cs^+(C_{10}H_8)_2$	0.014	0.006	0.046, 0.10	0.025, 0.035	0.0003

[a] Active external.
[b] Inactive external.
[c] Rotational constants of the transition state treated as free internal rotors.
[d] Two-dimensional rotational constant of the transition state at threshold, treated variationally and statistically.

2.3. Theoretical calculations

To obtain model structures, vibrational frequencies, rotational constants, and energetics for the neutral $C_{10}H_8$ ligand and for the $M^+(C_{10}H_8)_x$ complexes, ab initio and density functional theory calculations were performed using Gaussian 98 [54]. Geometry optimizations were performed at B3LYP/6-31G* level [55,56] for the $M^+(C_{10}H_8)_x$ complexes, where $M^+ = Li^+$, Na^+, and K^+. For complexes containing Rb^+ and Cs^+, geometry optimizations were performed using a hybrid basis set in which the effective core potentials (ECPs) and valence basis sets of Hay and Wadt were used to describe the metal ion [57], while 6-31G* basis sets were used for C and H atoms. As suggested by Glendening et al. [58], a single polarization (*d*) function was added to the Hay–Wadt valence basis set for Rb and Cs, with exponents of 0.24 and 0.19, respectively.

Vibrational analyses of the geometry-optimized structures were performed to determine the vibrational frequencies for the neutral $C_{10}H_8$ ligand and the $M^+(C_{10}H_8)_x$ complexes for $M^+ = Li^+$, Na^+, and K^+. The vibrational frequencies for the $Rb^+(C_{10}H_8)_x$ and $Cs^+(C_{10}H_8)_x$ complexes were estimated by scaling the frequencies for the analogous $K^+(C_{10}H_8)_x$ complexes using a procedure described in detail previously [59]. When used to model data or calculate thermal energy corrections, the calculated vibrational frequencies were pre-scaled by a factor of 0.9804 [60]. The vibrational frequencies and rotational constants of neutral $C_{10}H_8$ and all 10 $M^+(C_{10}H_8)_x$ complexes are listed in Tables 1 and 2, respectively. Single point energy calculations were performed at the MP2(full)/6-311+G(2d,2p) level using the B3LYP/6-31G* and B3LYP/Hybrid (6-31G*, Hay–Wadt) optimized geometries. To obtain accurate BDEs, zero-point energy (ZPE) corrections were applied and basis set superposition errors (BSSEs) were subtracted from the computed dissociation energies in the full counterpoise correction [61,62]. The ZPE and BSSE corrections decrease with increasing size of the alkali metal ion and range from 1.0 kJ/mol (Cs^+) to 6.6 kJ/mol (Li^+) and from 6.6 kJ/mol (Cs^+) to 20.3 kJ/mol (Li^+) across these systems, respectively.

3. Results

3.1. Cross-sections for CID

Experimental cross-sections were obtained for the interaction of Xe with the mono and bis $M^+(C_{10}H_8)_x$

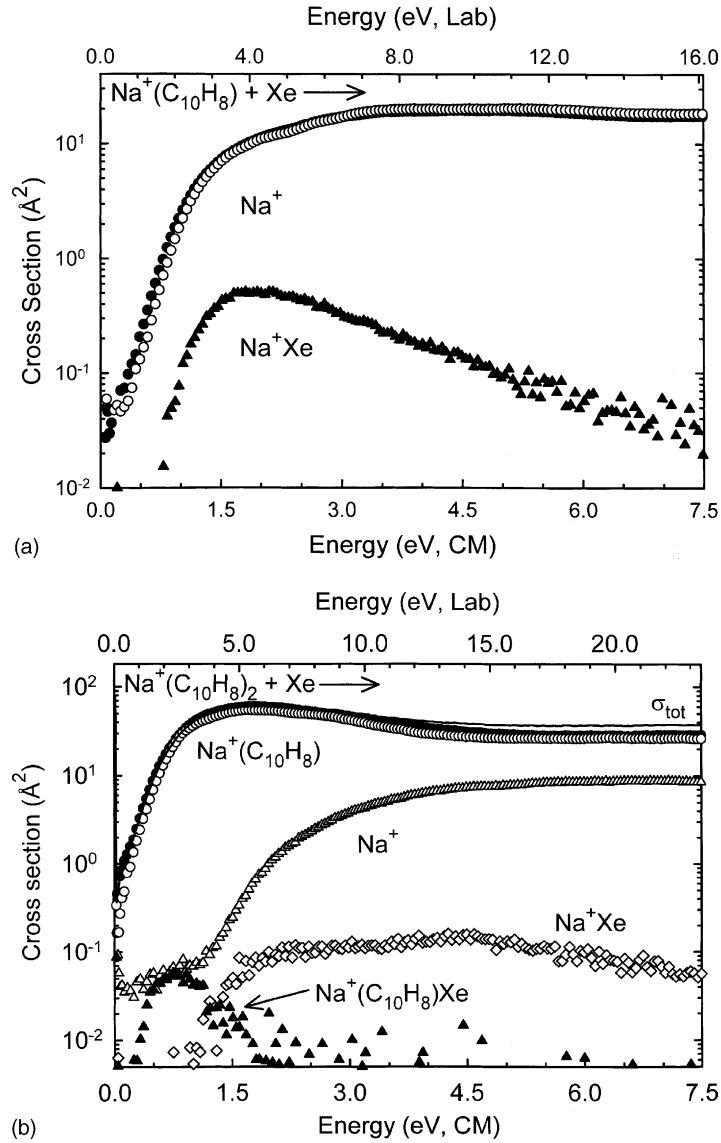

Fig. 1. Cross-sections for collision-induced dissociation of $Na^+(C_{10}H_8)_x$, $x = 1$ and 2 (panels a and b, respectively), with Xe as a function of kinetic energy in the center-of-mass frame (lower x-axis) and the laboratory frame (upper x-axis). Data are shown for a Xe pressure of ~0.2 and ~0.1 mTorr, for the $x = 1$ and 2 complexes, respectively. Primary and secondary product cross-sections are shown as (●) and (△), respectively. Primary and secondary ligand exchange product cross-sections are shown as (▲) and (◇), respectively. Data are also shown for the primary product cross-section, extrapolated to zero pressure of Xe, as (○).

complexes, where $M^+ = Li^+$, Na^+, K^+, Rb^+, and Cs^+. Fig. 1 shows representative data for the $Na^+(C_{10}H_8)_x$, $x = 1$ and 2 complexes. The behavior of the other $M^+(C_{10}H_8)_x$ complexes is quite similar to that observed for the $Na^+(C_{10}H_8)_x$ complexes. Over the collision energy range studied, 0 to >5 eV, only two types of processes are observed; simple CID resulting in loss of intact naphthalene molecules and ligand exchange with Xe. The most favorable process observed for all of the $M^+(C_{10}H_8)_x$ complexes is the

loss of a single intact naphthalene molecule in the CID reactions 2.

$$M^+(C_{10}H_8)_x + Xe \rightarrow M^+(C_{10}H_8)_{x-1} + C_{10}H_8 + Xe \quad (2)$$

In the $M^+(C_{10}H_8)$ complexes, the thresholds for reaction 2 decrease and the maximum cross-section increases with increasing size of the metal cation; behavior indicative of electrostatic binding. The $Rb^+(C_{10}H_8)$ and $Cs^+(C_{10}H_8)$ complexes deviate from this simple trend exhibiting a maximum cross-section intermediate between those observed for the Na^+ and K^+ complexes. The $M^+(C_{10}H_8)_2$ complexes exhibit similar behavior. The thresholds for reaction 2 again decrease and the maximum cross-section increases with increasing size of the metal cation. The $Rb^+(C_{10}H_8)_2$ and $Cs^+(C_{10}H_8)_2$ complexes also deviate from this simple trend exhibiting maximum cross-sections that are smaller than for the other alkali metal cations. This behavior is not well understood, but was also observed in other complexes to Rb^+ and Cs^+. The maximum cross-section for reaction 2, as well as the total cross-section, roughly doubles in magnitude from the mono to the bis complexes. The threshold for reaction 2 also decreases from the mono to the bis complexes, behavior that is again indicative of electrostatic binding. At elevated energies, sequential dissociation of a second naphthalene ligand is observed in the bis complexes. When this reaction pathway becomes energetically accessible, the cross-section for the primary CID product declines, indicating that loss of the second naphthalene ligand occurs sequentially rather than directly from the reactant complex.

Ligand exchange reactions to produce M^+Xe and $M^+(C_{10}H_8)Xe$ are also observed as minor reaction channels. The apparent thresholds for these processes decrease regularly as the size of the cation increases and are smaller for the bis complexes than for the mono complexes. The cross-section magnitudes of the primary and secondary ligand exchange products are very small and are ~1000–100 times smaller than the primary CID product, respectively.

3.2. Threshold analysis

The thresholds for reactions 2 in the $M^+(C_{10}H_8)_x$ complexes were modeled using Eq. (1). The results of these analyses are given in Table 3 for all 10 $M^+(C_{10}H_8)_x$ complexes. Representative fits using Eq. (1) for the $Na^+(C_{10}H_8)_x$ complexes are shown in Fig. 2. Accurate reproduction of the experimental cross-sections for the primary dissociation processes of the $M^+(C_{10}H_8)_x$ complexes is obtained using a loose PSL TS model [42]. This model has been shown to provide the most accurate determination of lifetime effects for CID reactions for electrostatically

Table 3
Fitting parameters of Eq. (1), threshold dissociation energies at 0 K, and entropies of activation at 1000 K[a]

Reactant complex	σ_0[b]	n[b]	E_0[c] (eV)	E_0(PSL) (eV)	Kinetic shift (eV)	$\Delta S^{\ddagger}$(PSL) (J/K/mol)
$Li^+(C_{10}H_8)$	1.3(0.3)	1.3(0.1)	2.40(0.17)	1.93(0.16)	0.47	41(2)
$Na^+(C_{10}H_8)$	18.8(1.0)	1.3(0.1)	1.12(0.06)	1.11(0.05)	0.01	38(3)
$K^+(C_{10}H_8)$	35.9(1.6)	1.2(0.1)	0.84(0.06)	0.84(0.05)	0.00	35(3)
$Rb^+(C_{10}H_8)$	7.9(2.4)	1.1(0.1)	0.76(0.06)	0.76(0.05)	0.00	43(5)
$Cs^+(C_{10}H_8)$	16.1(1.4)	1.2(0.1)	0.72(0.06)	0.72(0.05)	0.00	47(5)
$Li^+(C_{10}H_8)_2$	29.9(1.0)	0.9(0.1)	1.59(0.06)	1.21(0.04)	0.38	36(4)
$Na^+(C_{10}H_8)_2$	102.7(9.4)	1.0(0.1)	1.06(0.05)	0.94(0.03)	0.12	34(5)
$K^+(C_{10}H_8)_2$	68.0(8.3)	1.1(0.2)	0.82(0.07)	0.77(0.03)	0.05	18(5)
$Rb^+(C_{10}H_8)_2$	31.1(6.7)	0.9(0.1)	0.75(0.08)	0.72(0.04)	0.03	20(9)
$Cs^+(C_{10}H_8)_2$	53.6(6.4)	0.8(0.1)	0.70(0.10)	0.67(0.05)	0.03	21(9)

[a] Uncertainties are listed in parentheses.
[b] Average values for loose PSL transition state.
[c] No RRKM analysis.

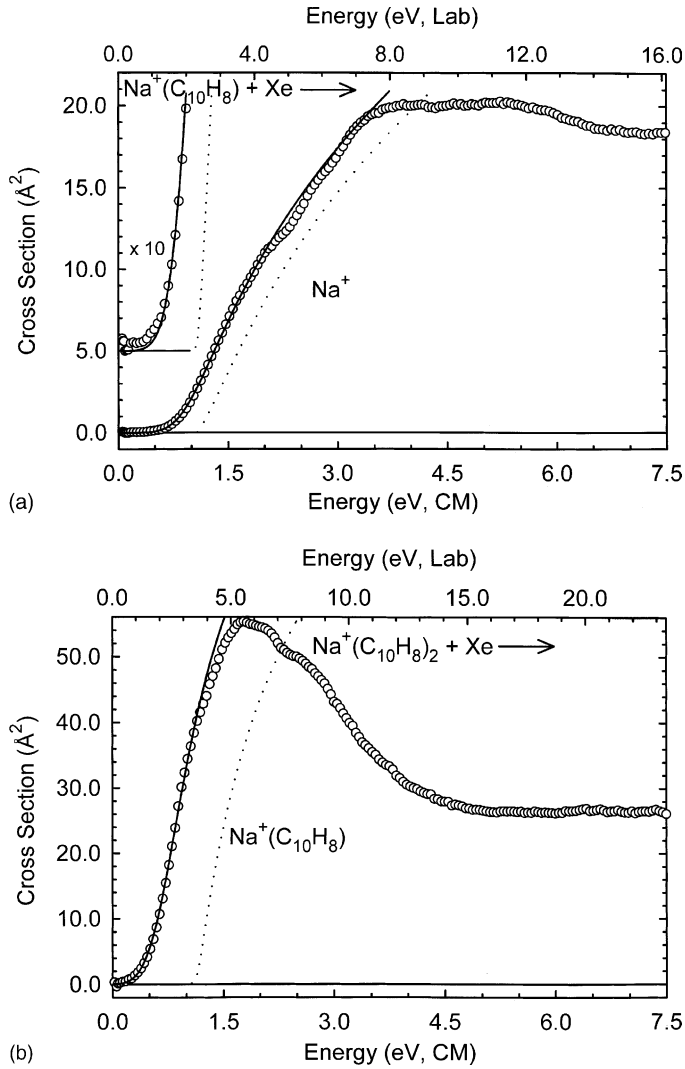

Fig. 2. Zero-pressure extrapolated cross-sections for the primary collision-induced dissociation product of the $Na^+(C_{10}H_8)_x$ complexes, $x = 1$ and 2 (panels a and b, respectively), with Xe in the threshold region as a function of kinetic energy in the center-of mass frame (lower x-axis) and the laboratory frame (upper x-axis). Solid lines show the best fits to the data using the model of Eq. (1) convoluted over the neutral and ion kinetic and internal energy distributions. Dashed lines show the model cross-sections in the absence of experimental kinetic energy broadening for reactants with an internal energy of 0 K.

bound metal–ligand complexes [42,63]. The data are accurately reproduced over energy ranges exceeding 1 eV and over cross-section magnitudes of at least a factor 100 for all complexes except $Rb^+(C_{10}H_8)_2$ and $Cs^+(C_{10}H_8)_2$. For these complexes, the primary CID cross-sections are already nonzero at 0 eV, so reproduction covers a more limited energy and magnitude range. Threshold values, E_0, obtained from analyses of the data without consideration of lifetime effects are also included in Table 3. The differences between these values and those obtained when lifetime effects are included E_0(PSL), the kinetic shifts, are also given in Table 3. The kinetic shifts decrease with increasing size of the cation, from Li^+ to Cs^+ for both the

Table 4
Enthalpies and free energies binding of $M^+(C_{10}H_8)_x$, $x = 1$–2 at 0 and 298 K in kJ/mol[a]

Reactant complex	ΔH_0[b]	$\Delta H_{298} - \Delta H_0$[c]	ΔH_{298}	$T\Delta S_{298}$[c]	ΔG_{298}
$Li^+(C_{10}H_8)$	187.2(16.4)	2.6(2.5)	189.8(12.2)	32.9(6.9)	156.9(14.1)
$Na^+(C_{10}H_8)$	107.1(5.0)	0.8(1.8)	107.9(5.3)	30.5(7.7)	77.4(9.3)
$K^+(C_{10}H_8)$	80.9(5.1)	0.3(1.5)	81.2(5.3)	28.9(7.8)	52.3(9.4)
$Rb^+(C_{10}H_8)$	73.0(4.9)	0.3(1.6)	73.3(5.1)	30.9(8.1)	42.4(9.6)
$Cs^+(C_{10}H_8)$	62.3(5.4)	0.3(1.4)	69.6(5.6)	31.8(8.5)	37.8(10.2)
$Li^+(C_{10}H_8)_2$	116.8(4.0)	−3.7(1.6)	113.1(4.3)	36.2(13.0)	76.9(13.7)
$Na^+(C_{10}H_8)_2$	91.1(2.5)	−3.4(1.5)	87.7(2.9)	35.7(13.3)	52.0(13.6)
$K^+(C_{10}H_8)_2$	74.7(3.4)	−3.7(1.1)	71.0(3.6)	31.3(13.4)	39.7(13.9)
$Rb^+(C_{10}H_8)_2$	69.6(4.0)	−3.7(1.1)	65.9(4.1)	31.5(14.7)	34.4(15.3)
$Cs^+(C_{10}H_8)_2$	65.1(3.4)	−3.7(1.1)	61.4(3.5)	31.9(14.9)	29.5(15.3)

[a] Uncertainties are listed in parentheses.
[b] Present experimental results, Table 3.
[c] Values from calculations at the B3LYP/6-31G* level of theory with frequencies scaled by 0.9804. The Hay–Wadt ECP/valence basis set was used for Rb^+ and Cs^+.

mono and the bis complexes. The mono complexes have 51 vibrational modes and only complexes to the most strongly bound metal cations, Li^+ and Na^+, exhibit kinetic shifts of 0.47 and 0.01 eV, respectively. The bis complexes have 105 vibrational modes and all of these complexes exhibit kinetic shifts of 0.38, 0.12, 0.05, 0.03, and 0.03 eV, respectively. As can be seen in Table 3, the observed kinetic shift directly correlates with the density of states of the complex at threshold, which depends upon the number of degrees of freedom and the measured BDE.

The entropy of activation, $\Delta S^{\dagger}$, is a measure of the looseness of the TS. It is largely determined by the molecular parameters used to model the energized molecule and the TS, but also depends upon the threshold energy. The $\Delta S^{\dagger}$(PSL) values at 1000 K are listed in Table 1 and vary between 18 and 47 J/K/mol. These entropies of activation compare favorably to an expanding range of noncovalently bound metal–ligand complexes previously measured in our laboratory and to those collected by Lifshitz for simple bond cleavage reactions of ions [64].

The 0 K bond energies determined here are also converted to 298 K bond enthalpies and free energies. Standard formulas assuming harmonic oscillator and rigid rotor models are used to calculate the enthalpic and entropic conversions using the vibrational and rotational constants determined for the B3LYP/6-31G* optimized geometries (Tables 1 and 2). Table 4 lists 0 and 298 K enthalpies, free energies, and enthalpic and entropic corrections for all systems experimentally determined (from Table 3). The uncertainties in the enthalpic and entropic corrections are determined by 10% variation in the molecular constants for complexes to Li^+, Na^+, and K^+, and by 20% variation in the molecular constants for complexes to Rb^+ and Cs^+. The listed uncertainties also include contributions from scaling the metal–ligand frequencies up and down by a factor of 2 because these low-energy modes may not be adequately described by theory. The latter is the dominant source of error in the uncertainties listed and provides a conservative estimate of the computational errors in these low-frequency modes.

3.3. Theoretical results

Theoretical structures for naphthalene and for the mono and bis complexes of naphthalene with Li^+, Na^+, K^+, Rb^+, and Cs^+ were calculated as described above. Details of the geometry-optimized structures for each of these species are given in Table 5. Two different conformers were calculated for each of the $M^+(C_{10}H_8)$ complexes, πr and πc. The geometry-optimized structures for the $Na^+(C_{10}H_8)$ complex are shown in Fig. 3. Two different conformers were also calculated for each of the $M^+(C_{10}H_8)_2$

Table 5
Geometrical parameters of B3LYP/6-31G* optimized structures of the $M^+(C_{10}H_8)_x$ complexes[a]

Complex	Conformer	M^+–C[b] (Å)	M^+–ring-centroid[c] (Å)	M^+–centroid[d] (Å)	C–C (Å)	C–H (Å)	CHOOP∠[e] (°)
$C_{10}H_8$					1.415	1.088	0.000
$Li^+(C_{10}H_8)$	πr	2.336	1.858	2.227	1.423	1.087	0.114
	πc		2.418	2.088	1.411	1.087	0.177
$Na^+(C_{10}H_8)$	πr	2.745	2.352	2.652	1.423	1.087	0.160
	πc		2.750	2.464	1.410	1.087	0.218
$K^+(C_{10}H_8)$	πr	3.176	2.842	3.094	1.420	1.087	0.267
	πc		3.154	2.909	1.407	1.087	0.178
$Rb^+(C_{10}H_8)$[f]	πr	3.459	3.146	3.375	1.419	1.087	0.130
	πc		3.411	3.185	1.409	1.087	0.163
$Cs^+(C_{10}H_8)$[f]	πr	3.690	3.363	3.577	1.417	1.087	1.097
	πc		3.644	3.434	1.408	1.087	0.151
$Li^+(C_{10}H_8)_2$	πa	2.505	2.064	2.400	1.410	1.087	0.090
	πs	2.505	2.063	2.398	1.410	1.087	0.090
$Na^+(C_{10}H_8)_2$	πa	2.826	2.442	2.731	1.409	1.087	0.114
	πs	2.823	2.441	2.730	1.409	1.087	0.098
$K^+(C_{10}H_8)_2$	πa	3.230	2.902	3.149	1.408	1.087	0.108
	πs	3.230	2.907	3.153	1.408	1.087	0.108
$Rb^+(C_{10}H_8)_2$[f]	πa	3.500	3.196	3.421	1.408	1.087	0.128
	πs	3.500	3.206	3.430	1.408	1.087	0.128
$Cs^+(C_{10}H_8)_2$[f]	πa	3.775	3.487	3.695	1.408	1.087	0.100
	πs	3.785	3.522	3.727	1.408	1.087	0.099

[a] Average values are provided when small variations in the bond distances and angles exist.
[b] The M^+–C distance is the distance from the metal cation to the carbon atoms within the aromatic ring of naphthalene over which the metal cation resides.
[c] M^+–ring-centroid distance is defined as the distance from the metal cation to the central point within the aromatic ring of naphthalene over which the metal cation resides.
[d] The M^+–centroid distance is defined as the distance from the metal cation to the centroid of the naphthalene molecule.
[e] Out-of-plane angle.
[f] The Hay–Wadt ECP/valence basis set was used for the metal ion, as described in the text.

complexes, πa and πs. The geometry-optimized structures for the $Na^+(C_{10}H_8)_2$ complex are shown in Fig. 4.

In the πr conformer, the metal cation sits above the center of one of the aromatic rings of the naphthalene molecule and binds to the π cloud of that aromatic ring. In the πc conformer, the metal cation sits above the center of the naphthalene molecule again binding to the π cloud of the aromatic system. The πr conformers are calculated to be true minima on the $M^+(C_{10}H_8)$ potential energy surface. In contrast, the πc conformers are found to be TS structures with the single imaginary frequency corresponding to motion of the metal cation oscillating along the direction connecting the two equivalent πr structures. The πc conformers were found to be 22.2, 5.9, and 1.7 kJ/mol less stable than the corresponding πr conformers for the $M^+(C_{10}H_8)$ complexes to Li^+, Na^+, and K^+, respectively. Oddly enough, the calculations find that the πc conformers for the $M^+(C_{10}H_8)$ complexes to Rb^+ and Cs^+ are 2.5 and 0.8 kJ/mol more stable than the πr conformers, respectively. This is indeed unexpected because the πr conformers are found to be true minima with no imaginary frequencies for all five metal cations, and the πc conformers are found to be the TS structures that join the two equivalent minima. However, the above energetics are based upon single point energy calculations performed at the MP2(full)/6-311+G(2d,2p) level of theory, whereas the optimizations were carried out at the B3LYP/6-31G* level of theory. If the relative sta-

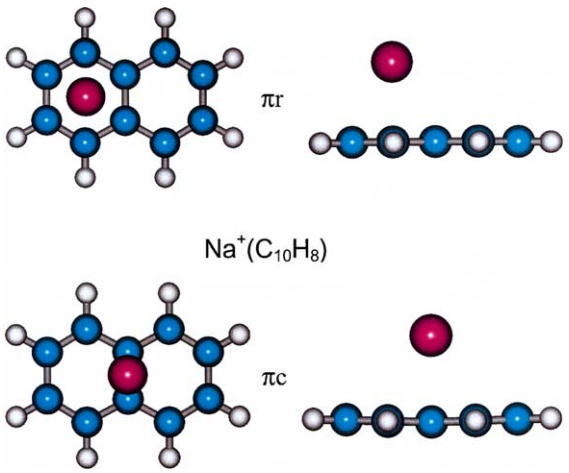

Fig. 3. B3LYP/6-31G* optimized geometry of $Na^+(C_{10}H_8)$ π complex. Two views of each conformer, πr (ground state) and πc (transition state), are shown.

bilities of the πr and πc conformers of the Rb^+ and Cs^+ complexes are compared at the B3LYP/6-31G* level of theory, the πr conformers are indeed more stable than the πc TS conformers by 1.6 and 0.5 kJ/mol, respectively. In any event, it is clear that at room temperature all of the $M^+(C_{10}H_8)$ complexes should have sufficient internal energy to traverse the barrier separating the two equivalent πr conformations except the $Li^+(C_{10}H_8)$ complex (Table 1).

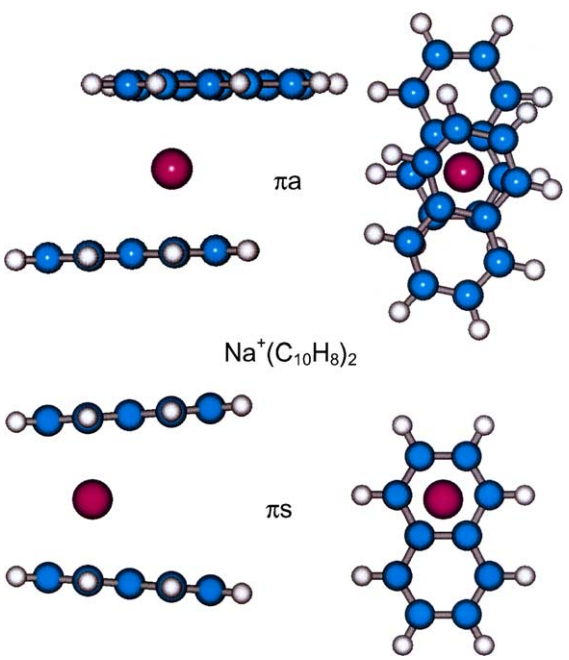

Fig. 4. B3LYP/6-31G* optimized geometries of $Na^+(C_{10}H_8)_2$ π complexes. Two views of each conformer, πa and πs, are shown.

The distortion of the naphthalene molecule that occurs upon complexation to the alkali metal cation is minor. The change in geometry is largest for the complex to Li^+ and decreases with increasing size of the metal cation. In the πr conformers, the C–C bond lengths of the aromatic rings of naphthalene were found to increase by 0.002–0.008 Å upon complexation to the alkali metal cation as compared to the free ligand (Table 5). In contrast, the C–C bond lengths of the aromatic rings of naphthalene were found to decrease by 0.005–0.008 Å upon complexation to the alkali metal cation in the πc conformers (Table 2). The aromatic C–H bond lengths decrease from 1.088 to 1.087 Å upon complexation. As summarized in Table 5, M^+–C, M^+–ring-centroid, and M^+–centroid distances[1] are found to increase as the size of the metal ion increases. These distances are also found to increase on going from the mono to the corresponding bis complexes. It is interesting to note that the M^+–ring-centroid distance in the πr conformer is always shorter than the M^+–centroid distance in the corresponding πc conformer. In a previous study of the $Na^+(C_{10}H_8)$ π complex performed by Dunbar [40], two stable conformations very similar to the πr and πc conformers were also found. Consistent with the results found here, the Na^+–ring-centroid distance of the πr conformer, 2.37 Å, is shorter than the Na^+–centroid distance of the πc conformer, 2.48 Å. Both of these distances are 0.02 Å longer than corresponding lengths found in the present work. Out-of-plane bending of the ring H atoms is found to decrease with increasing size of the metal cation for both the mono and bis complexes. Further, out-of-plane bending of the

[1] The metal ring-centroid distance is defined as the distance from the metal cation to the central point within the plane of the aromatic ring that the cation is directly interacting with. The metal centroid distance is defined as the distance from the metal cation to the centroid of the naphthalene molecule.

ring hydrogen atoms is smaller than for the analogous benzene complexes [26]. Likewise, out-of-plane bending is smaller for the bis complexes than for the mono complexes. This makes sense because the alkali metal cation is further away from the ring in the complexes to naphthalene than it is in the complexes to benzene. Likewise, the alkali metal cation is further away from the ring in the bis complexes than it is in the mono complexes. The longer M^+–ring-centroid distance results in the metal ion exerting a smaller influence on the ligand. Similar trends were observed in the analogous cation-π complexes to other aromatic ligands previously studied in our laboratory [29–32,34].

As can be seen in Fig. 4 for the $Na^+(C_{10}H_8)_2$ complex, the πa conformer has the Na^+ ion sandwiched between the aromatic rings that are directly binding to the metal cation. The naphthalene molecules are nearly parallel and oriented "skewed" anti to one another. Repulsive interactions between the terminal H atoms of one naphthalene ligand and aromatic ring of the other ligand cause the rings to skew. In contrast, the rings were always aligned in the stable structures found for the other cation-π bis complexes we have examined [29,30–34]. We also found stable structures for all of the $M^+(C_{10}H_8)_2$ in which the metal cation is sandwiched between aligned naphthalene ligands. Repulsive interactions between the aromatic rings not directly interacting with the metal cation cause the naphthalene ligands to fan out from a parallel conformation. The deviations from parallel are largest for the Li^+ complex and decrease with increasing size of the metal cation, such that the dihedral angle between the planes of the two naphthalene ligands ranges from 9.0° (Li^+) to 2.8° (Cs^+). It is interesting to note that the stability of these two conformations is very similar for all of the alkali metal cations examined here. The relative stability of these conformations of the $M^+(C_{10}H_8)_2$ complexes, hereafter referred to as πa, the "skewed" anti conformation, and πs, the fanned out aligned conformation, varies with the metal cation. The πa conformers are more stable for Na^+ and Rb^+; whereas the πs conformers are more stable for Li^+, K^+, and Cs^+. In all cases the difference in stability is small and <3.5 kJ/mol. Therefore, at room temperature these complexes should have sufficient energy to freely interconvert (see Table 1). In addition, it is likely that other stable conformers of the $M^+(C_{10}H_8)_2$ complexes in which the naphthalene ligands are rotated between the two limiting conformations found here exist and are of very similar stability. Because the barrier to interconversion of the two equivalent πr mono conformers is small and the relative stabilities of the bis conformers are very similar, it is probably most appropriate to think of the $M^+(C_{10}H_8)_x$ complexes as highly dynamic clusters with the metal cation interacting with the entire aromatic system rather than being localized at a specific site on the molecule.

Theoretical estimates for the $M^+(C_{10}H_8)_x$ BDEs were determined using the B3LYP/6-31G* geometries and single point energy calculations at MP2(full)/6-311+G(2d,2p). In earlier work in which we measured and calculated the strength of cation-π interactions in $M^+(toluene)_x$ complexes [29], we found much better correlation between the theoretical and experimental results for energetics based on MP2(full)/6-311+G(2d,2p) theory than for B3LYP/6-311+G(2d,2p) theory and have, therefore, employed the former in the present study. To obtain accurate BDEs, ZPE and BSSE corrections have also been included. These results are listed in Table 6 along with other theoretical results found in literature [39,40].

4. Discussion

4.1. Trends in experimental $M^+(C_{10}H_8)_x$ BDEs

The 0 K experimental BDEs of the $M^+(C_{10}H_8)_x$ complexes are also summarized in Table 6. The variation in the measured BDEs with the size of the alkali metal cation is shown in Fig. 5 for both the mono and bis complexes. The M^+–$(C_{10}H_8)$ and $(C_{10}H_8)M^+$–$(C_{10}H_8)$ BDEs are found to decrease monotonically as the size of the metal cation increases from Li^+ to Cs^+. Similar trends were observed for the analogous cation-π complexes to other aromatic ligands previously studied in our laboratory [29–32,34] as well as those to benzene determined

Table 6
Bond dissociation enthalpies of $M^+(C_{10}H_8)_x$, $x = 1$–2 at 0 K in kJ/mol

Complex	Experiment (TCID)		Conformer	Theory (L = $C_{10}H_8$)			D_e
	L = $C_{10}H_8$[a]	L = C_6H_6[b]		D_e[c]	D_0[c,d]	$D_{0,BSSE}$[c,e]	
Li^+(L)	187.2(16.4)	161.1(13.5)	πr	172.9	166.3	155.8	
			πc	147.6	143.4	133.6	
Na^+(L)	107.1(5.0)	92.6(5.8)	πr	116.0	112.7	101.5	120.1[f]
		88.3(4.3)[g]					129.7[h]
			πc	109.2	106.6	95.6	121.3[h]
K^+(L)	80.9(5.1)	73.3(3.8)	πr	92.2	89.7	83.1	
			πc	90.6	88.5	81.4	
Rb^+(L)[i]	73.0(4.9)	68.5(3.8)	πr	79.6	77.1	66.1	
			πc	80.1	78.4	68.6	
Cs^+(L)[i]	69.3(5.4)	64.6(4.8)	πr	74.4	71.9	61.2	
			πc	74.7	72.0	62.0	
$Li^+(L)_2$	116.8(4.0)	104.2(6.8)	πa	137.2	135.3	115.0	
			πs	140.4	138.5	116.2	
$Na^+(L)_2$	91.1(2.5)	80.0(5.8)	πa	106.1	105.1	87.1	
			πs	105.4	102.9	83.6	
$K^+(L)_2$	74.8(3.4)	67.5(6.8)	πa	84.7	81.5	69.4	
			πs	84.8	82.8	71.0	
$Rb^+(L)_2$[i]	69.6(4.0)	62.7(7.7)	πa	80.3	78.8	64.5	
			πs	78.6	77.2	62.6	
$Cs^+(L)_2$[i]	65.1(3.3)	58.8(7.7)	πa	67.3	66.3	54.8	
			πs	67.6	66.7	55.5	

[a] Present results, threshold collision-induced dissociation. Uncertainties are listed in parenthesis.
[b] Taken from Amicangelo and Armentrout [26], except as noted.
[c] Calculated at the MP2(full)/6-311+G(2d,2p) level of theory using B3LYP/6-31G* optimized geometries.
[d] Including zero-point energy corrections with B3LYP/6-31G* frequencies scaled by 0.9804.
[e] Also includes basis set superposition error corrections.
[f] Mecozzi et al. [39] calculated at the HF/6-31G**//HF/6-31G** level of theory.
[g] Armentrout and Rodgers [25].
[h] Dunbar [40] calculated at HF/6-31G* level of theory.
[i] The Hay–Wadt ECP/valence basis set was used for the metal ion, as described in the text.

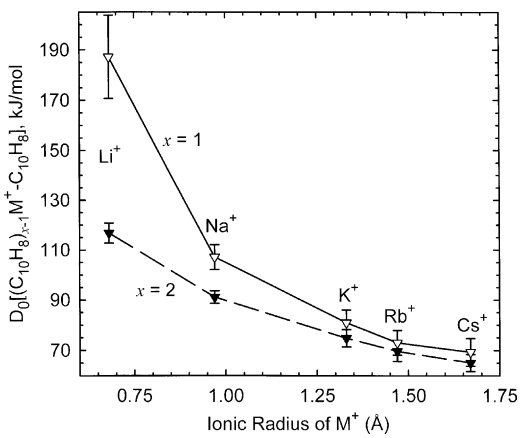

Fig. 5. Bond dissociation energies at 0 K (in kJ/mol) of the $M^+(C_{10}H_8)_x$ complexes plotted vs. the ionic radius of M^+. Data are shown for $x = 1$ and 2 as (▽) and (▼), respectively. All values are taken from Table 3.

by Amicangelo and Armentrout [26]. This behavior supports the conclusion that these complexes are non-covalently bound. The BDE decreases with increasing size of the alkali metal cation because the distance between the alkali metal cation and the aromatic ligand becomes larger (see Table 5), and the electrostatic interactions are expected to fall off rapidly with distance. An ion-quadrupole interaction is expected to exhibit an R^{-3} distance dependence, whereas an ion-induced dipole interaction is expected to exhibit an R^{-4} distance dependence. However, these distance dependencies assume that the cation does not perturb the electron density of the π ligand, which would only be true for very large distances. Thus, it is not expected that the trends measured here should closely follow these distance dependences. The distance de-

pendence of the cation-π interactions examined here fall off at a much more rapid rate of $R^{-1.5}$ for the mono complexes. The distance dependence of the cation-π interactions in the bis complexes exhibits an even more rapid rate of fall off of $R^{-1.1}$. This more rapid fall off is the result of the repulsive Coulombic interactions between the two π ligands in the bis complexes. A Coulombic interaction is expected to exhibit an R^{-1} distance dependence. Thus, it is clear that an accurate description of the cation-π interaction must take into consideration the interaction of the ion with the full electrostatic potential surface of the π ligand as previously suggested [1,2,20].

The BDEs of the bis complexes are smaller than the corresponding mono complexes in all cases. The decrease in the measured BDE on going from the mono to the corresponding bis complex is largest for Li^+, and decreases with increasing size of the alkali metal cation. The sequential BDE is found to decrease by 70.4, 16.0, 6.1, 3.4, and 4.2 kJ/mol for the Li^+, Na^+, K^+, Rb^+, and Cs^+ systems, respectively. Similar trends were observed for the analogous cation-π complexes to other aromatic ligands previously studied in our laboratory [29–32,34] as well as those to benzene [26]. Coulombic repulsions between the ligands fall off as the distance between the ligands increases [63]. The distance between the naphthalene ligands increases with increasing size of the metal cation, from ∼4.12 Å in $Li^+(C_{10}H_8)_2$ to 6.97 Å in $Cs^+(C_{10}H_8)_2$, (Table 5, $2\times M^+$–ring-centroid distance of the πa conformers). The increasing separation of the ligands with increasing size of the metal cation leads to smaller repulsive ligand–ligand interactions and, therefore, smaller differences in the sequential BDEs as the size of the metal cation increases. The ligand–ligand repulsions appear to be very small for the complexes to K^+, Rb^+, and Cs^+ resulting in very small differences between the BDEs in the mono and bis complexes (Table 6).

4.2. Comparison of theory and experiment

The experimentally determined and theoretically calculated $M^+(C_{10}H_8)_x$ BDEs are listed in Table 6.

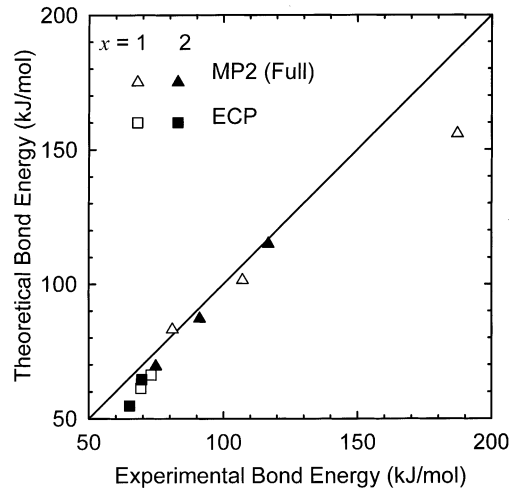

Fig. 6. Theoretical vs. experimental bond dissociation energies at 0 K (in kJ/mol) of the $M^+(C_{10}H_8)_x$ complexes. The diagonal line indicates the values for which the calculated and measured bond dissociation energies are equal. All values are taken from Table 3.

The agreement between the experimental and theoretical BDEs determined at MP2(full)/6-311+G(2d,2p)//B3LYP/6-31G* level is illustrated in Fig. 6. As can be seen in the figure, the agreement between theory and experiment is very good for the Li^+, Na^+, and K^+ complexes, where full electron correlation is included except for the $Li^+(C_{10}H_8)$ complex. Somewhat less satisfactory agreement is found for the Rb^+ and Cs^+ complexes, where ECPs are employed. The absolute accuracy of the levels of theory used here can be gauged by examining the mean absolute deviation (MAD) between the experimental and theoretical values. The MAD for all 10 complexes is 8.3 ± 8.6 kJ/mol; somewhat larger than the average experimental error of 5.4 ± 4.0 kJ/mol. The MAD is larger for the mono complexes, 10.8 ± 11.7 kJ/mol, than for the bis complexes, 5.7 ± 3.5 kJ/mol. The agreement between the experimental and six theoretical $M^+(C_{10}H_8)_x$ BDEs calculated, including all electrons ($M^+ = Li^+$, Na^+, K^+, $x = 1$ and 2), is reasonably good, with a MAD of 8.5±11.5 kJ/mol; again somewhat larger than the average experimental error in these values, 6.1 ± 5.2 kJ/mol. The large difference between theoretical BDE and the experimental

value for $Li^+(C_{10}H_8)$, 31.4 kJ/mol, is disappointing. If this value is not included, the MAD drops to 3.9 ± 2.7 kJ/mol which compares well with average experimental error of 4.0±1.1 kJ/mol. The poor agreement for the $Li^+(C_{10}H_8)$ complex may arise for two reasons. One is the experimental difficulty associated with efficient detection of Li^+ [43]. An alternative possibility is that theory may systematically underestimate the bond energies for Li^+ complexes, as a result of the higher degree of covalency in the metal–ligand bond. This is shown by the calculated partial charge on M^+, which is 0.79*e* for $Li^+(C_{10}H_8)$ and varies between 0.89 and 0.99*e* for all other $M^+(C_{10}H_8)_x$, complexes. Therefore, higher levels of theory may be required to accurately describe the binding in this complex, a conclusion also drawn for Li^+ complexes with a variety of other ligands [28,29,43,65,66].

The agreement between the experimental BDEs and the theoretical values calculated using the Hay–Wadt ECP/valence basis set for the Rb^+ and Cs^+ complexes is also reasonably good. A MAD of 7.9 ± 1.3 kJ/mol is found; twice as large as the average experimental error in these values, 4.0 ± 1.0 kJ/mol. Consistent with the analogous cation-π complexes to other aromatic ligands previously studied in our laboratory [29–32,34] as well as those to benzene [26], the Hay–Wadt ECP/valence basis set provides calculated BDEs that are reasonably accurate, but systematically lower than the experimental values.

Dougherty and coworkers [39] calculated the binding energy (D_e) for the $Na^+(C_{10}H_8)$ complex at the HF/6-31G**//HF/6-31G** level of theory to be 120.1 kJ/mol, 4.1 kJ/mol higher than that calculated here. The inclusion of ZPEs is obviously important as their value is 18.6 and 13.0 kJ/mol higher than the D_0 values calculated and measured here, respectively. Dunbar [40] estimated the D_e's of the πr and πc conformers of the $Na^+(C_{10}H_8)$ complex at MP2/6-31G**//HF/6-31G* level of theory to be 121.3 and 129.7 kJ/mol, respectively. In their study, they were more interested in mapping the potential energy surface for binding over the entire face than obtaining accurate absolute BDEs. Thus, their absolute BDEs are too high because ZPE and BSSE corrections were not included and because a frozen HF geometry for the naphthalene ligand was employed. The difference in stability of the πr and πc conformers found by Dunbar, 8.4 kJ/mol, is very similar to that found here 6.8 kJ/mol. These comparisons make it obvious that determination of accurate theoretical BDEs must include ZPE corrections, whereas the need to include BSSE corrections is highly dependent upon the level of theory employed and is more important for ab initio calculations than for density functional calculations. The higher level of theory employed in the present work provides a BDE for $Na^+(C_{10}H_8)$ of 101.5 kJ/mol, in very good agreement with the measure value, 107.1 ± 5.0 kJ/mol.

4.3. The influence of the extended π network

The effect of the additional aromatic ring of naphthalene on the cation-π interaction can be examined by comparing the results obtained here for naphthalene to those obtained in previous studies of benzene [26] and a variety of substituted benzenes: toluene, aniline, phenol, anisole, and fluorobenzene [29–32,34]. In these earlier studies, we found that the influence of a substituent on the strength of the cation-π interaction could be understood by considering the change in the quadrupole moment (or π-electron density) and polarizability of the aromatic ligand induced by the substituent. In all of the cation-π complexes previously studied, except those to aniline, the dipole moment of the aromatic ligand lies in the plane of the aromatic ring and, therefore, an effective interaction of the alkali metal cation with the dipole moment is not possible. Therefore, the ion-dipole interaction enhances the strength of the binding in the cation-π complexes to aniline compared to that observed for the other aromatic ligands, where the ion-dipole interaction is ineffective or absent.

As can be seen in Fig. 7, naphthalene binds more strongly than benzene in all cases. The increase in the strength of the cation-π interaction can be understood by examining the influence of the extended π network on the quadrupole moment and polarizability. Like benzene, naphthalene possesses a center of

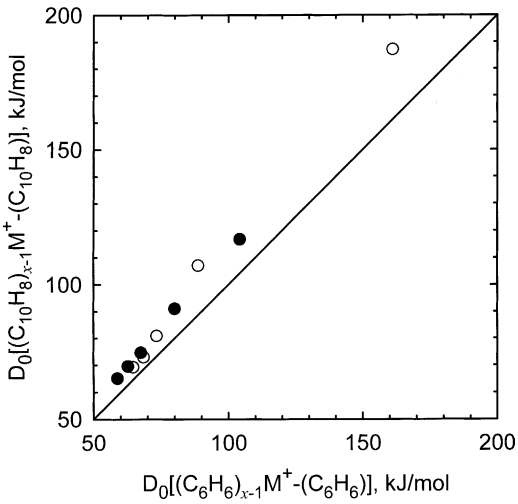

Fig. 7. Experimental bond dissociation energies (in kJ/mol) at 0 K of the $(C_{10}H_8)_{x-1}M^+$–$(C_{10}H_8)$ vs. $(C_6H_6)_{x-1}M^+$–(C_6H_6), where $M^+ = Li^+$, Na^+, K^+, Rb^+, and Cs^+ and $x = 1$ (○) and 2 (●). Values for C_6H_6 are taken from Amicangelo and Armentrout [26]. The diagonal line indicates the values for which the bond dissociation energies to naphthalene and benzene are equal.

symmetry and has no dipole moment. Therefore, the ion-dipole interaction has no effect on the strength of the binding in the cation-π complexes to naphthalene or benzene. The delocalized π-electron density above and below the aromatic ring results in a quadrupole moment for benzene of −8.69 DÅ [67]. However, the quadrupole moment of naphthalene has not been reported. Benzene has 6 π-electrons equally distributed over 6 C atoms, whereas naphthalene has 10 π-electrons symmetrically, but not quite equally, distributed over 10 carbon atoms. Although naphthalene has 67% more π-electron density than benzene, that electron density is delocalized over nearly twice the volume. Thus, it is expected that the quadrupole moment of naphthalene is roughly equal to that of benzene. Therefore, the extended π network is not expected to enhance the ion-quadrupole interaction in the cation-π complexes to naphthalene compared to that observed for benzene. The additivity method of Miller [68] provides estimated polarizabilities of 9.99 $Å^3$ for benzene and 17.59 $Å^3$ for naphthalene. Therefore, the ion-induced dipole interaction should be ∼76% stronger in naphthalene than in benzene. As discussed above, the binding in the cation-π complexes to naphthalene is expected to be largely electrostatic, arising form ion-dipole, ion-quadrupole, and ion-induced dipole interactions, but dominated by the ion-quadrupole interaction. The center of symmetry eliminates the ion-dipole contribution to the binding. The ion-quadrupole interaction should be roughly as strong as that to benzene, and the ion-induced dipole interaction should be stronger than to benzene. The increase in the cation-π BDEs to naphthalene, relative to those of benzene varies between 4.5 and 26.1 kJ/mol for the mono complexes and 6.3 and 12.6 kJ/mol for the bis complexes (Table 6). This corresponds to an average increase in the strength of the binding of ∼14%. The absolute enhancement in binding is greatest for the Li^+ complexes and decreases with increasing size of the cation. Likewise, the absolute enhancement in binding is greater for the mono complexes than for the bis complexes of Li^+, Na^+, K^+, but is slightly smaller for Rb^+ and Cs^+.

A crude estimate of the relative contributions of the ion-quadrupole and ion-induced dipole interactions to the binding in cation-π complexes to benzene and naphthalene can be obtained by comparing the BDEs and assuming that the difference represents ∼76% of the ion-induced dipole contribution in the benzene complexes. This simple analysis suggests that the bonding is indeed dominated by the ion-quadrupole interaction, which accounts for ∼79–91% of the overall bond strength in the complexes to benzene and ∼68–86% in the complexes to naphthalene. This requires that the alkali metal cation–ligand bond distances be very similar in the $M^+(C_6H_6)_x$ and $M^+(C_{10}H_8)_x$ complexes, as verified by theoretical calculations. The relative ion-induced dipole contribution to the binding is larger for the smaller cations, Li^+ and Na^+, than for the larger metal cations because of the R^{-4} dependence of this interaction, vs. the R^{-3} dependence of the ion-quadrupole interaction.

This simple analysis can be carried further by comparing the BDEs determined for the substituted benzenes, toluene [29], aniline [31], phenol [32], anisole [34], and fluorobenzene [30], to those of ben-

zene [26]. In this way, the relative contributions of the ion-quadrupole and ion-induced dipole interactions to the binding in the substituted benzenes can be assessed and used to provide a rough estimate of the quadrupole moment of these ligands. Because the binding in the complexes to aniline also involves contributions from the ion-dipole interaction, the relative contributions of the ion-dipole and ion-quadrupole interactions in these complexes cannot be separated. This too requires that the alkali metal cation–ligand bond distances be very similar in the $M^+(C_6H_6)_x$ and $M^+(C_6H_5X)_x$ complexes, as verified by theoretical calculations. Again we find that the ion-quadrupole interaction dominates the binding in these complexes, contributing ~73–91% of the overall bonding in the complexes to toluene, aniline, phenol, anisole, and fluorobenzene. Rough estimates of the quadrupole moments of these ligands of -9.1 ± 0.4, $\leq -10.0 \pm 0.4$, -8.8 ± 0.4, -9.0 ± 0.4, -8.5 ± 0.4, and -6.4 ± 0.5 DÅ are obtained, respectively. The estimated quadrupole moment of aniline of -10.0 ± 0.4 DÅ represents an upper limit because the ion-dipole and ion-quadrupole contributions to the binding cannot be separated. These estimated quadrupole moments agree with qualitative and semi-quantitative predictions of the influence of the substituent on the π-electron density of the aromatic ring as discussed previously [29–32,34]. Future studies of other π ligands might also help deduce the relative contributions of the ion-dipole and ion-quadrupole interactions in aniline.

4.4. Comparison to other $M^+(C_{10}H_8)$ complexes

As mentioned in Section 1, studies of cation-π interactions of other metal cations with naphthalene have been very limited. In an ab initio mapping study of the binding of Na^+, Mg^+, and Al^+ to the π faces of naphthalene and indole, Dunbar [40] calculated binding energy profiles of these cations along the molecular long axis of these molecules at the HF/6-31G* level of theory. For each metal cation, he found a double well potential with a small barrier separating two stable equivalent conformations. The geometries of the minima and saddle point he found are similar to the πr and πc conformers of the mono complexes found here. The calculated BDEs of these complexes increase from Na^+ to Mg^+ then decrease to Al^+ and are 129.7, 188.3, and 179.9 kJ/mol, respectively. As discussed above, these values are expected to be overestimates based on the level of theory employed and the neglect of ZPE and BSSE corrections. The binding to Mg^+ and Al^+ is much stronger than to Na^+ as a result of the contribution of the valence electrons and sp-polarization effects to the binding in the complexes to the former ions [69]. The barrier to interconversion of the two πr conformations, i.e., the difference in stability of the πr and πc conformers, increases from Na^+ to Mg^+ to Al^+ and is 8.4, 16.7, and 20.9 kJ/mol, respectively. As discussed above, these values are expected to be reasonably accurate.

In the study of the radiative association reactions of Si^+, Fe^+, Cr^+, and Mn^+ with naphthalene, Dunbar and coworkers observed the formation of both mono and bis complexes to each of these cations, except Si^+, where only the mono complex was formed. In addition, they determined lower limits to the binding energies of naphthalene to Si^+ and Fe^+ of 174 kJ/mol for both ions. This value is greater than the BDEs measured here for all of the alkali metal cations except Li^+. The large BDEs to these cations result from the contributions to the binding in these complexes from the valence electrons and sp-polarization and sd-hybridization effects [69].

5. Conclusions

The kinetic energy dependences of the CID of $M^+(C_{10}H_8)_x$ complexes, where $M^+ = Li^+$, Na^+, K^+, Rb^+, and Cs^+, and $x = 1$ and 2, with Xe are examined in a guided ion beam tandem mass spectrometer. The dominant dissociation pathway observed for all complexes is loss of an intact naphthalene ligand. Thresholds for these primary dissociation reactions are determined after careful consideration of the effects of reactant internal energy, multiple collisions with Xe, and the lifetime of the ionic reactants (using a loose PSL TS model). The molecular parameters needed for the analysis of experimental

data as well as structures and theoretical estimates of the BDEs for the $M^+(C_{10}H_8)_x$ complexes are obtained from theoretical calculations performed at the MP2(full)/6-311+G(2d,2p)//B3LYP/6-31G(d) level of theory. The absolute M^+–$(C_{10}H_8)$ and $(C_{10}H_8)M^+$–$(C_{10}H_8)$ BDEs are observed to decrease monotonically as the size of the alkali metal ion increases from Li^+ to Cs^+. Similarly, the difference in the BDEs for the mono and bis complexes is also observed to decrease with the size of the alkali metal cation. These trends are explained in terms of the electrostatic nature of the bonding in the $M^+(C_{10}H_8)_x$ complexes and the changes in magnitude of the ligand–ligand interactions in the $M^+(C_{10}H_8)_2$ complexes, respectively. Theoretical values of the $M^+(C_{10}H_8)_x$ BDEs are also determined by ab initio calculations performed at the MP2(full)/6-311+G(2d,2p)//B3LYP/6-31G(d) level of theory. The agreement between experiment and theory is very good for all complexes except for the $Li^+(C_{10}H_8)$ complex.

Comparisons made to other alkali metal cation-π complexes previously studied reveal that cation-π interactions are indeed dominated by the ion-quadrupole interaction, which contributes ∼68–91% to the overall binding interaction. Ion-induced dipole interactions also contribute to the binding, and to a greater extent in complexes to the smallest cations as expected on the basis of the distance dependences of the ion-quadrupole and ion-induced dipole interactions. Further, the extended π network of naphthalene leads to an increase in the strength of the cation-π interaction, in both the mono and bis complexes, to all of the alkali metal cations. The enhanced binding observed in the naphthalene systems, compared to that observed for benzene, results from the increased polarizability of the ligand because the extended π network does not significantly change the quadrupole moment.

Acknowledgements

This work was supported by the National Science Foundation Grant No. CHE-0138504.

References

[1] J.C. Ma, D.A. Dougherty, Chem. Rev. 97 (1997) 1303.
[2] D.A. Dougherty, Science 271 (1996) 163.
[3] H. Nicholson, W.J. Becktel, B.W. Matthews, Nature 336 (1988) 651.
[4] J. Sancho, L. Serrano, A.R. Fersht, Biochemistry 31 (1992) 2253.
[5] S.K. Burley, G.A. Petsko, Science 34 (1985) 15301.
[6] L. Serrano, M. Bycroft, A.R. Fersht, J. Mol. Biol. 218 (1991) 465.
[7] J. Sunner, K. Nishizawa, P. Kebarle, J. Phys. Chem. 85 (1981) 1814.
[8] C.A. Deakyne, M. Meotner, J. Am. Chem. Soc. 107 (1985) 474.
[9] M. Meotner, C.A. Deakyne, J. Am. Chem. Soc. 107 (1985) 469.
[10] B.C. Guo, J.W. Purnell, A.W. Castleman, Chem. Phys. Lett. 168 (1990) 155.
[11] O.M. Carbarcos, C.J. Weinheimer, J.M. Lisy, J. Chem. Phys. 108 (1998) 5151.
[12] A.M. DeVos, M. Ultsch, A.A. Kossiakoff, Science 255 (1992) 306.
[13] A. Karlin, Curr. Opin. Neurobiol. 3 (1993) 299.
[14] M.L. Raves, M. Harel, Y.P. Pang, I. Silman, A.P. Kozikowski, J.L. Sussman, Nat. Struct. Biol. 4 (1997) 57.
[15] D.A. Stauffer, A. Karlin, Biochemistry 33 (1994) 6840.
[16] J.B. Mitchell, C.L. Nandi, I.K. McDonald, J.M. Thornton, S.L. Price, J. Mol. Biol. 239 (1994) 315.
[17] W. Zhong, J.P. Gallivan, Y. Zhang, L. Li, H.A. Lester, D.A. Dougherty, Proc. Natl. Acad. Sci. U.S.A. 95 (1998) 12088.
[18] O. Donini, D.F. Weaver, J. Comput. Chem. 19 (1998) 1515.
[19] R.L. Nakamura, J.A. Anderson, R.F. Gaber, J. Biol. Chem. 272 (1997) 1011.
[20] D.A. Dougherty, H.A. Lester, Angew. Chem. Int. Ed. Engl. 37 (1998) 2329.
[21] G.W. Gokel, S.L. De Wall, E.S. Meadows, Eur. J. Org. Chem. (2000) 2967.
[22] S.J. Lippard, J.M. Berg (Eds.), Principles of Bioinorganic Chemistry, University Science Books, Mill Valley, CA, 1994.
[23] R.L. Woodin, J.L. Beauchamp, J. Am. Chem. Soc. 100 (1978) 501.
[24] R.W. Taft, F. Anvia, J.-F. Gal, S. Walsh, M. Capon, M.C. Holmes, K. Hosn, G. Oloumi, R. Vasanwala, S. Yazdani, Pure Appl. Chem. 62 (1990) 17.
[25] P.B. Armentrout, M.T. Rodgers, J. Phys. Chem. A 104 (2000) 2238.
[26] J.C. Amicangelo, P.B. Armentrout, J. Phys. Chem. A 104 (2000) 11420.
[27] A. Gapeev, C.-Y. Yang, S.J. Klippenstein, R.C. Dunbar, J. Phys. Chem. A 104 (2000) 3246.
[28] H. Huang, M.T. Rodgers, J. Phys. Chem. A 106 (2002) 4277.
[29] R. Amunugama, M.T. Rodgers, J. Phys. Chem. A 106 (2002) 5529.
[30] R. Amunugama, M.T. Rodgers, J. Phys. Chem. A 106 (2002) 9092.

[31] R. Amunugama, M.T. Rodgers, Int. J. Mass Spectrom., in press.
[32] R. Amunugama, M.T. Rodgers, J. Phys. Chem. A 106 (2002) 9718.
[33] V. Ryzhov, R.C. Dunbar, J. Am. Chem. Soc. 121 (1999) 2259.
[34] R. Amunugama, M.T. Rodgers, Int. J. Mass Spectrom. 222 (2003) 431.
[35] V. Ryzhov, R.C. Dunbar, B. Cerda, C. Wesdemiotis, J. Am. Soc. Mass Spectrom. 11 (2000) 1037.
[36] A. Gapeev, R.C. Dunbar, J. Am. Chem. Soc. 123 (2001) 8360.
[37] D. Feller, D.A. Dixon, J.B. Nicholas, J. Phys. Chem. A 104 (2000) 11414.
[38] S. Tsuzuki, M. Yoshida, T. Uchimaru, M. Mikami, J. Phys. Chem. A 105 (2001) 769.
[39] S. Mecozzi, A.P. West Jr., D.A. Dougherty, J. Am. Chem. Soc. 118 (1996) 2307.
[40] R.C. Dunbar, J. Phys. Chem. A 102 (1998) 8946.
[41] R.C. Dunbar, G.T. Uechi, B. Asamoto, J. Am. Chem. Soc. 116 (1994) 2466.
[42] M.T. Rodgers, K.M. Ervin, P.B. Armentrout, J. Chem. Phys. 106 (1997) 4499.
[43] M.T. Rodgers, J. Phys. Chem. A 105 (2001) 2374.
[44] E. Teloy, D. Gerlich, Chem. Phys. 4 (1974) 417;
D. Gerlich, Diplomarbeit, University of Freiburg, Federal Republic of Germany, 1971;
D. Gerlich, in: C.-Y. Ng, M. Baer (Eds.), State-Selected and State-to-State Ion-Molecule Reaction Dynamics, Part I, Experiment, Adv. Chem. Phys. 82 (1992) 1.
[45] K.M. Ervin, P.B. Armentrout, J. Chem. Phys. 83 (1985) 166.
[46] N.F. Dalleska, K. Honma, L.S. Sunderlin, P.B. Armentrout, J. Am. Chem. Soc. 116 (1994) 3519.
[47] F. Muntean, P.B. Armentrout, J. Chem. Phys. 115 (2001) 213.
[48] T.S. Beyer, D.F. Swinehart, Comm. Assoc. Compt. Machines 16 (1973) 379;
S.E. Stein, B.S. Rabinovitch, J. Chem. Phys. 58 (1973) 2438;
S.E. Stein, B.S. Rabinovitch, Chem. Phys. Lett. 49 (1977) 1883.
[49] J.A. Pople, H.B. Schlegel, K. Ragavachari, D.J. DeFrees, J.F. Binkley, M.J. Frisch, R.F. Whitesides, R.F. Hout, W.J. Hehre, Int. J. Quant. Chem. Symp. 15 (1981) 269;
D.J. DeFrees, A.D. McLean, J. Chem. Phys. 82 (1985) 333.
[50] F.A. Khan, D.E. Clemmer, R.H. Schultz, P.B. Armentrout, J. Phys. Chem. 97 (1993) 7978.
[51] W.J. Chesnavich, M.T. Bowers, J. Phys. Chem. 83 (1979) 900.
[52] N.F. Dalleska, K. Honma, P.B. Armentrout, J. Am. Chem. Soc. 115 (1993) 12125 (see, for example, Fig. 1).
[53] P.B. Armentrout, J. Simons, J. Am. Chem. Soc. 114 (1992) 8627.
[54] M.J. Frisch, G.W. Trucks, H.B. Schlegel, G.E. Scuseria, M.A. Robb, J.R. Cheeseman, V.G. Zakrzewski, J.A. Montgomery Jr., R.E. Stratmann, J.C. Burant, S. Dapprich, J.M. Millam, A.D. Daniels, K.N. Kudin, M.C. Strain, O. Farkas, J. Tomasi, V. Barone, M. Cossi, R. Cammi, B. Mennucci, C. Pomelli, C. Adamo, S. Clifford, J. Ochterski, G.A. Petersson, P.Y. Ayala, Q. Cui, K. Morokuma, D.K. Malick, A.D. Rabuck, K. Raghavachari, J.B. Foresman, J. Cioslowski, J.V. Ortiz, B.B. Stefanov, G. Liu, A. Liashenko, P. Piskorz, I. Komaromi, R. Gomperts, R.L. Martin, D.J. Fox, T. Keith, M.A. Al-Laham, C.Y. Peng, A. Nanayakkara, C. Gonzalez, M. Challacombe, P.M.W. Gill, B. Johnson, W. Chen, M.W. Wong, J.L. Andres, C. Gonzales, M. Head-Gordon, E.S. Replogle, J.A. Pople, Gaussian 98, Revision A.11, Gaussian, Inc., Pittsburgh PA, 1998.
[55] A.D. Becke, J. Chem. Phys. 98 (1993) 5648.
[56] C. Lee, W. Yang, R.G. Parr, Phys. Rev. B 37 (1988) 785.
[57] P.J. Hay, W.R. Wadt, J. Chem. Phys. 82 (1985) 299.
[58] E.D. Glendening, D. Feller, M.A. Thompson, J. Am. Chem. Soc. 116 (1994) 10657.
[59] D. Walter, P.B. Armentrout, J. Am. Chem. Soc. 120 (1998) 3176.
[60] J.B. Foresman, ´Æ. Frisch, Exploring Chemistry with Electronic Structure Methods, 2nd ed., Gaussian, Pittsburgh, 1996, p. 64.
[61] S.F. Boys, R. Bernardi, Mol. Phys. 19 (1979) 553.
[62] F.B. Van Duijneveldt, J.G.C.M. van Duijneveldt-van de Rijt, J.H. van Lenthe, Chem. Rev. 94 (1994) 1873.
[63] M.T. Rodgers, P.B. Armentrout, J. Phys. Chem. A 101 (1997) 1238.
[64] C. Lifshitz, Adv. Mass Spectrom. 11 (1989) 113.
[65] M.T. Rodgers, P.B. Armentrout, J. Am. Chem. Soc. 122 (2000) 8548.
[66] M.T. Rodgers, J. Phys. Chem. A 105 (2001) 8145.
[67] J.H. Williams, Acc. Chem. Res. 26 (1993) 593.
[68] K.J. Miller, J. Am. Chem. Soc. 112 (1990) 8533.
[69] M.T. Rodgers, J.R. Stanley, R. Amunugama, J. Am. Chem. Soc. 122 (2000) 10969.